

Applications of Wavelets in Morphometric Analysis of Medical Images

Christos Davatzikos¹, Xiaodong Tao^{1,2}, and Dinggang Shen¹

¹Section for Biomedical Image Analysis, Department of Radiology, University of Pennsylvania, PA 19104

²Department of Electrical and Computer Engineering, Johns Hopkins University, Baltimore, MD 21218
{christos, dgshen}@rad.upenn.edu; xtao@iron.ece.jhu.edu

ABSTRACT

Morphometric analysis of medical images is playing an increasingly important role in understanding brain structure and function, as well as in understanding the way in which these change during development, aging and pathology. This paper presents three wavelet-based methods with related applications in morphometric analysis of magnetic resonance (MR) brain images. The first method handles cases where very limited datasets are available for the training of statistical shape models in the deformable segmentation. The method is capable of capturing a larger range of shape variability than the standard active shape models (ASMs) can, by using the elegant spatial-frequency decomposition of the shape contours provided by wavelet transforms. The second method addresses the difficulty of finding correspondences in anatomical images, which is a key step in shape analysis and deformable registration. The detection of anatomical correspondences is completed by using wavelet-based attribute vectors as morphological signatures of voxels. The third method uses wavelets to characterize the morphological measurements obtained from all voxels in a brain image, and the entire set of wavelet coefficients is further used to build a brain classifier. Since the classification scheme operates in a very-high-dimensional space, it can determine subtle population differences with complex spatial patterns. Experimental results are provided to demonstrate the performance of the proposed methods.

Keywords: Wavelet transform, morphological analysis, active shape model, attribute vector, morphological classification

1. INTRODUCTION

Morphometric analysis of brain changes provides the ability to better understand the effect of these factors on the brain structures, and has the potential to permit early diagnosis of diseases when effective treatments are still possible [1-8]. With the advent of modern imaging techniques, morphometric analysis is no longer conducted using histological methods on a limited number of subjects. Instead, population analysis based on large databases of images is used. This poses some challenges to the research community: Firstly, human brains, even normal ones, exhibit large inter-subject variability in structures. Secondly, the structural differences of the brains between different groups of people (i.e., people with and without a certain disease) are usually subtle. In order to find and quantify these subtle differences, it requires a good image registration method that is able to align individual brain images into a standardized reference space for increasing the sensitivity of the statistical analysis.

Wavelets have been applied with great success to a wide range of signal/image processing and analysis problems, such as signal compression [9], de-noising [10] and pattern recognition [11], since wavelets are well localized in both space and frequency domains. In this paper, three wavelet-based methods are presented for improving the performance of the segmentation, registration, and morphometric analysis algorithms in processing brain images. The first method, called *hierarchical active shape model* (hierarchical ASM), is proposed to address the problems that the statistical shape models face when very limited training datasets are available. The method is capable of capturing a larger range of shape variability than the standard active shape models (ASMs) can, by using the elegant spatial-frequency decomposition of the shape contours provided by wavelet transforms. Experimental results show that hierarchical ASM performs substantially better than the standard ASM even in cases where as few as 5 training samples are used to model a two-dimensional (2D) contour represented by 512 landmark points. In shape analysis and deformable registration of brain images, finding correspondence in anatomical images is a key step. Our second wavelet-based method investigates a technique of using wavelet-based attribute vectors as morphological signatures of some anatomically distinctive voxels for finding anatomical correspondences [12]. As wavelets are able to characterize the subtle anatomical differences in

the brain images, the anatomical correspondences can be accurately established by using wavelet-based anatomical representations. The third method uses the wavelets to hierarchically characterize the morphological measurements obtained from all voxels in a brain, and further use the entire set of wavelet coefficients for brain classification [13]. This differs from the voxel- and deformation-based morphometry (VBM and DBM) that have become common approaches to computational anatomy during the past several years. VBM and DBM are based on a spatial transformation that places images in a stereotaxic space, followed by a voxel-wise statistical analysis of the spatial distribution of different tissues (VBM) [14] or of the properties of the spatial transformation itself (DBM) [15].

Three wavelet-based methods will be described separately in the following three sections. Owing to space constraints, we will detail only the first method of deformable brain segmentation, and briefly introduce the main concepts in the other two methods.

2. HIERARCHICAL ACTIVE SHAPE MODELS USING WAVELET DECOMPOSITION

Deformable shape models have played an important role in the medical image analysis literature during the past 15 years. They have been used for segmentation and deformable registration of biomedical images. Typically deformable shape models impose some form of local smoothness constraint [16] via elastic forces or some combination of local and global constraints [17]. However, elastic models are often too flexible, and they can be trapped by spurious edges or by edges adjacent to the structure of interest, thus converging to a suboptimal, and often very poor, solution. Some of the limitations of deformable shape models were overcome by models that impose constraints not pertaining to some physical model (e.g., elastic), but rather to a statistical shape model derived from a training set. In [18,19] a frequency-based model was proposed, and in [20] a model using principal component analysis (PCA) was used. Other investigators subsequently used these models with some success [21-26]. Active shape models (ASMs) certainly mitigated the problem of local minima, by restricting the possible configurations a deformable shape can assume. However, they themselves suffer from a fundamental limitation: They often restrict the deformable shape too much, particularly if they have been trained on a relatively small number of samples. This is because the number of eigenvectors that can be used to represent any shape is at most equal to the number of training samples minus one, whereas the number of points comprising the shape might be two or more orders of magnitude higher. In other words, it is difficult to estimate a high-dimensional probability distribution of a shape from a relatively small number of samples. As a result, the subspace of “allowable shapes” spanned by the relatively few eigenvectors limits the ability of an ASM to follow the fine details of a shape. Here, we describe a new method for building the statistical shape model for planar shapes based on multi-resolution representation of the deformable contours. We use wavelet decomposition of the coordinates of the landmark points of training shapes to build hierarchical active shape models and apply the models for segmentation of callosal boundaries in the midsagittal sections of MR images of human brains. A hierarchical formulation of ASMs allows our model to capture both the global shape characteristics and the fine local details, thereby overcoming current limitations of ASMs.

2.1 Methods

Assume that N training samples are available in the form of sets of K corresponding landmarks in the D -dimensional space. Assume, also, that standard Procrustes alignment [27] has been performed on the training samples to eliminate the variations introduced by translation, scaling, and rotation. Let the vectors $\mathbf{x}_n, n=1, \dots, N$, be formed by concatenating the coordinates of the K landmark points of the n -th sample. Let $\mathbf{e}_1, \dots, \mathbf{e}_{N-1}$ be the eigenvectors corresponding to the non-zero eigenvalues of the covariance matrix, \mathbf{C} , calculated from these vectors. (There could, in principle, be fewer than $N-1$ eigenvectors with non-zero eigenvalues, but this is rarely the case when only a limited number of samples is available, which is the focus of our paper.) If, as is typically the case, $N \ll D \cdot K$, it is likely that the space, \mathbf{S} , spanned by $\mathbf{e}_1, \dots, \mathbf{e}_{N-1}$, does not represent the full range of shape variation one expects to find in biomedical images. Therefore, in a standard ASM, which includes a step in which tentative shapes are projected onto \mathbf{S} , final shape reconstructions often appear to lack fine details. Clearly, the more samples available, the larger \mathbf{S} is, and the more faithful the shape reconstructions.

Assume, now, that we are only interested in representing a segment of a shape, comprising K' points, rather than the whole shape (see Fig. 1). If K' is small enough, then N samples will be adequate to represent the variability of that segment, thus allowing the model to locally capture the fine details of the segment. This would be achieved, however, at the expense of disregarding spatial relationships between points of that segment and points of other segments of the shape. Such relationships can be captured by a statistical prior relating the positions of the segments relative to each other. For example, one can apply a standard ASM on the centers of mass of these segments. This is one of the simplest forms of a hierarchical ASM [28].

A more formal framework is the wavelet decomposition of a contour or surface representing the shape, followed by estimation of the statistics of the resulting expansion coefficients. Because wavelets are well localized in both space and frequency domains, they are suitable for representing local frequency components in a given signal. The wavelet transform provides an elegant way to perform a scale-space decomposition. In the context of this work, we use a logarithm tree 2-band wavelet packet to divide the space-frequency domain. For a p level wavelet packet, we divide the frequency domain into $B = 2^p$ frequency bands (see Fig. 2).

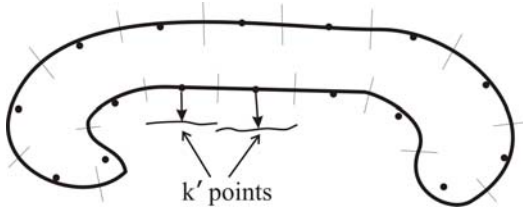


Figure 1. A contour can be partitioned into smaller segments. The global shape characteristics can be captured by a statistical prior relating the centers of mass (solid circles) of all segments. Finer and local shape characteristics can be captured by statistical priors for each segment individually. When the global prior is used to reposition the center of mass points, the respective segments are repositioned rigidly by the same displacement vector. This might lead to discontinuities. In order to remedy this situation, we use overlapping segments, with a continuous blending.

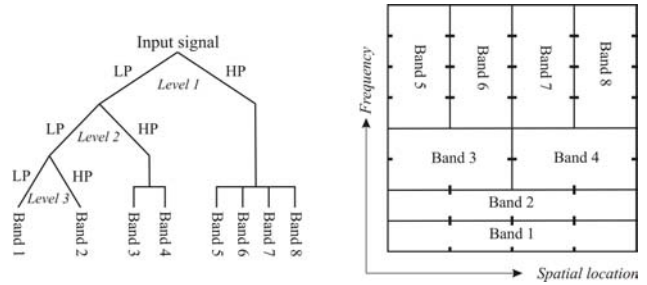


Figure 2. Three-level logarithm tree 2-band wavelet packet. The wavelet transform is iterated for the lowpass branches (marked as LP in the figure). The outputs of the highpass branches (marked as HP in the figure) are divided into a number of bands. The number of bands for each highpass branch is determined by the level at which the highpass filtering is performed. In this way, for a p level wavelet decomposition the frequency domain is divided into $B = 2^p$ bands. The space-frequency domain partition of the signal is shown on the right.

2.1.1 Analysis steps using wavelet transform

Now let us consider the wavelet transform of the deformable contours. As stated before, we assume that N training samples are available in the form of sets of K corresponding landmarks. Assume that the x -, y -coordinates of the k -th landmark of the n -th training sample after Procrustes alignment are (u_{nk}, v_{nk}) , $n = 1, \dots, N$ and $k = 1, \dots, K$. Then each training sample can be represented by its x -, y -coordinate vectors:

$$\begin{aligned} \mathbf{u}_n &= [u_{n1}, u_{n2}, \dots, u_{nK}]^T \\ \mathbf{v}_n &= [v_{n1}, v_{n2}, \dots, v_{nK}]^T, \quad n = 1, \dots, N \end{aligned}$$

By applying wavelet transform to \mathbf{u}_n and \mathbf{v}_n , we get their wavelet coefficients:

$$\mathbf{c}_n = W[\mathbf{u}_n] = [c_{ni}, i = 1, \dots, L] \quad (1)$$

$$\mathbf{d}_n = W[\mathbf{v}_n] = [d_{ni}, i = 1, \dots, L] \quad (2)$$

where $W(\bullet)$ denotes the wavelet decomposition. Note that \mathbf{c}_n and \mathbf{d}_n are not necessarily K dimensional vectors. Their dimension, L , depends on what scaling/wavelet functions we use in the transform. In this paper, we use a p -level logarithm tree 2-band wavelet packet to divide the digital frequency domain into $B = 2^p$ bands (see Fig. 2). In particular, $p = 6, B = 64$. By using the wavelet transform, large i 's in Equations (1) and (2) correspond to high frequency

information (local shape information), while small i 's carry relatively lower frequency information (global shape information). Moreover, the index i is related to the spatial location along the contour, around which shape information is collected.

Let $\mathbf{w}_n = [c_{n1}, d_{n1}, c_{n2}, d_{n2}, \dots, c_{nL}, d_{nL}]^T$ be the $2L \times 1$ vector formed by concatenating the wavelet coefficients of the n -th subject. We divide the vectors $\mathbf{w}_1, \dots, \mathbf{w}_N$ into $B = 64$ bands each. Let $\mathbf{w}_n^{(b)}$ be the wavelet coefficient vector for band $b, n = 1, \dots, N, b = 1, \dots, B$. We calculate the inter-individual variation of the wavelet coefficients within each band (see Fig. 2) from vectors $\mathbf{w}_n^{(b)}$. The complete statistical shape model includes the mean and covariance matrix of wavelet coefficients for each band:

$$\begin{aligned} \boldsymbol{\mu}^{(b)} &= \frac{1}{N} \sum_{n=1}^N \mathbf{w}_n^{(b)} \\ \mathbf{C}^{(b)} &= \frac{1}{N-1} \sum_{n=1}^N (\mathbf{w}_n^{(b)} - \boldsymbol{\mu}^{(b)})(\mathbf{w}_n^{(b)} - \boldsymbol{\mu}^{(b)})^T \end{aligned}$$

We then perform PCA in each band individually, thus obtaining 64 sets of eigenvectors and eigenvalues. Let $\Phi^{(b)}$ be the matrix formed by the eigenvectors for the wavelet coefficients of the b -th band and $\Lambda^{(b)}$ be the vector of the eigenvalues of the wavelet coefficients of the b -th band. The eigenvectors and eigenvalues of the first few bands represent relatively global aspects of shape variability, whereas bands with higher indices represent higher frequency and more localized aspects of shape variability. Each band has a relatively small number of variables, compared to the total number of points. Moreover, these variables form a fairly compact distribution, since they tend to be correlated. Therefore, its eigenvectors span a relatively large subspace. In this way, the overconstraining effect of standard ASMs is overcome.

2.1.2 Reconstruction of the contour from the wavelet coefficients

With the eigenvectors and eigenvalues for each of the B bands, $\Phi^{(b)}$, and $\Lambda^{(b)}$, $b = 1, \dots, B$, we can approximate any new shapes by projecting the wavelet coefficients of each band to the corresponding eigen space, and thus reconstruct the plausible shapes. Suppose a new shape, \mathbf{a} , is represented by a list of landmark points (u_k, v_k) , $k = 1, \dots, K$. We approximate \mathbf{a} using the statistical shape model as follows:

- 1) Align \mathbf{a} with the mean shape in the model using appropriate translation, scaling, and rotation to get $\mathbf{T}(\mathbf{a})$;
- 2) Apply the wavelet transform $W(\bullet)$ to the x - and y -coordinate vectors of $\mathbf{T}(\mathbf{a})$ to get the wavelet coefficients \mathbf{c} and \mathbf{d} (Equations (1) and (2));
- 3) Divide \mathbf{c} and \mathbf{d} into B bands each using the same partition of the space-frequency domain used in building the model. The coefficient vector for each band is $\mathbf{s}^{(b)}, b = 1, \dots, B$;
- 4) Approximate $\mathbf{s}^{(b)}$ using the statistical shape model as:

$$\hat{\mathbf{s}}^{(b)} = \boldsymbol{\mu}^{(b)} + \Phi^{(b)} q_b,$$

where q_b is a parameter vector computed by truncating each component of $\Phi^{(b)T} \cdot (\mathbf{s}^{(b)} - \boldsymbol{\mu}^{(b)})$ with two standard deviations of corresponding eigen variation for the b -th band;

- 5) Group $\hat{\mathbf{s}}^{(b)}, b = 1, \dots, B$ into wavelet coefficients $\hat{\mathbf{c}}$ and $\hat{\mathbf{d}}$, and use inverse wavelet transform to reconstruct the shape $\hat{\mathbf{a}}$;
- 6) Apply the inverse of the transform in Step 1) to get $\tilde{\mathbf{a}} = \mathbf{T}^{-1}(\hat{\mathbf{a}}) = (\tilde{u}_k, \tilde{v}_k)$, $k = 1, \dots, K$, which is the projection of \mathbf{a} onto the model space.

2.2 Results

2.2.1 Deformable segmentation on midsagittal sections of MR brain images

We applied the standard active shape model (ASM) and the hierarchical active shape model (hierarchical ASM) to the midsagittal sections of MR images of human brains to find the callosal boundaries. We randomly selected midsagittal sections from our database of normal elderly subjects participating in the Baltimore Longitudinal Study of Aging [2]. The training set was built by having an expert outline the callosal boundary, and specifying two landmark points, namely the anterior-most and posterior-most tips of the callosum along its axis of symmetry. Training contours were then parameterized by piece-wise constant speed parameterizations in between landmarks. Each contour was represented by 512 landmark points. Fig. 3 shows some examples for callosal boundaries.

In order to compare the performance of different models, we used the same initialization and the same deformation scheme for the models. During the deformation, each landmark point was moved to its nearby feature in the image. And this displacement was propagated to its neighbors according to a Gaussian fall-off function in order to achieve a smooth deformation. After all landmark points were moved according to the image features, the tentative contour was mapped to the shape space (constrained by two standard deviations from the mean in the direction of each eigenvector) to initialize the next iteration. The iterative deformation was terminated when the difference between two successive iterations was sufficiently small.

We first tested the standard ASM for different numbers of training samples. The images are 256×256 pixels in size. Fig. 4 shows a test image on the left, and the results obtained using standard ASMs trained on 99, 50, 20, 10 and 5 samples. Although for an adequately large number of samples a good segmentation was obtained, the segmentation error increased rapidly when fewer than 50 samples were used.

We then used the 5 samples of Fig. 3 to train our hierarchical ASM. Fig. 5 shows three examples of segmentations obtained using standard ASM and hierarchical ASM. It is clear that standard ASM needs to be trained on a sufficiently large number of samples in order to capture the finer details of individual shapes, which is not the case with hierarchical ASM.

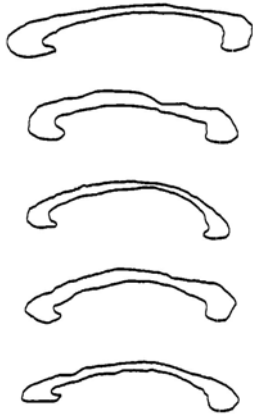


Figure 3. Five representative training samples used in the experiments of this paper.

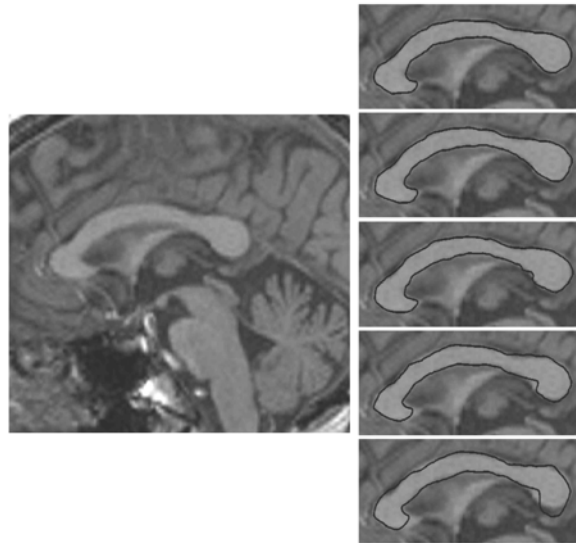


Figure 4. (Left) Midsagittal MR image. (Right) Automated segmentation obtained using the standard ASM trained on 99, 50, 20, 10, and 5 samples (top to bottom, respectively). The standard ASM performs well when enough training samples are available, relative to the variability of the structure, but starts to fail when relatively few training samples are available.

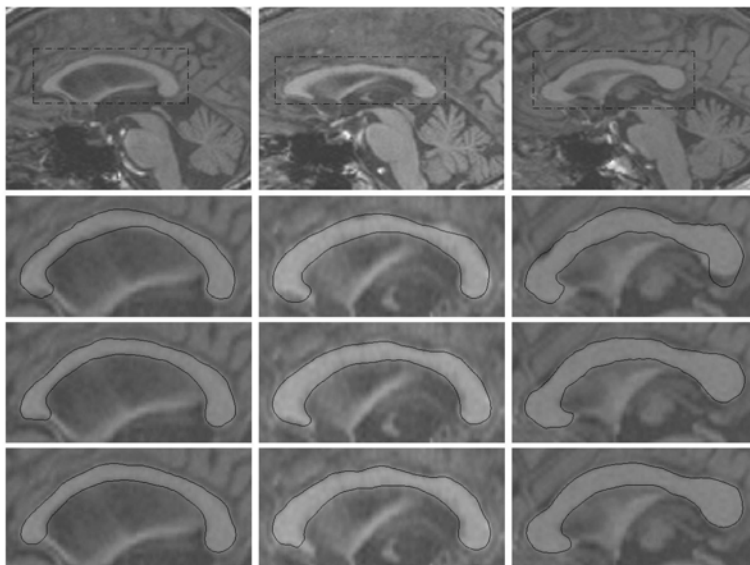


Figure 5. Top row: midsagittal images of the corpus callosum of three subjects. Second to fourth rows: segmentations obtained using standard ASM trained on 5 samples, standard ASM trained on 99 samples, hierarchical ASM trained on 5 samples. It is clear that standard ASM needs to be trained on a sufficiently large number of samples in order to capture the finer details of individual shapes, which is not the case with the hierarchical ASM.

2.2.2 Quantitative analysis of the methods

In this experiment, we applied standard ASMs and hierarchical ASM, trained on different numbers of training samples, to the midsagittal sections of MR images of eight human brains, and computed the errors of the resulting contours using different shape models by comparing them with the corresponding contours manually outlined by the human expert. The error is calculated by averaging the distance from the points on a contour to the closest point on the contours outlined manually by the human expert. Table 1 shows the average errors of the eight callosal boundaries.

Table 1. Average errors between the results using different models trained on different number of training samples and the corresponding boundaries manually drawn by the human expert. Numbers in the table are in pixels.

Method	<i>Number of training samples</i>									
	5	10	15	20	30	40	50	65	80	99
Standard ASM	2.26	2.11	2.07	1.99	1.99	2.03	1.90	1.95	1.91	1.90
Hierarchical ASM	1.97	1.95	1.93	1.94	1.94	1.94	1.91	1.93	1.92	1.91

3. CORRESPONDENCE DETECTION USING WAVELET-BASED ATTRIBUTE VECTORS

Finding point correspondence in anatomical images is a key step in shape analysis and deformable registration. If the anatomical correspondences between the brain template and the individual brains can be established correctly for all voxels by a correspondence-detection algorithm, then the task of aligning the individuals to the template can be completed immediately. This section briefly describes an automatic correspondence detection algorithm using wavelet-based attribute vectors defined on every image voxel [12]. The attribute vector reflects the anatomical characteristics in a large neighborhood around the respective voxel. It plays the role of a morphological signature for each voxel and is therefore made as distinctive as possible. Correspondence is then determined by evaluating the similarities of attribute vectors.

In our method, the voxel-wise attribute vectors are designed for correspondence detection in a multi-resolution framework. The attribute vector of a voxel reflects the anatomy in the vicinity of that voxel, thus it should be calculated from the image data within a neighborhood of the voxel. For each voxel, the discrete wavelet transformation [9] of the

image data within a sliding window centered on that voxel is performed, which yields a series of subimages, and the feature images are formed by combining these wavelet subimages. The wavelet-based attribute vector is finally constructed from the feature images. Although a wavelet-based attribute vector is not rotation-invariant, it can tolerate a small rotation angle, and it gives detailed representation of anatomical features around a voxel. In practice, some rigid registration methods can be used initially if the rotational angle between two brains is large. Then the wavelet-based attribute vectors can be further applied to determine the correspondences. To speed up the algorithm, the wavelet-based correspondence detection algorithm is also implemented in a multi-resolution fashion. That is, the correspondences are first established in the low-resolution images, then refined in the higher-resolution images.

We tested this wavelet-based correspondence detection method on hundreds of voxels from images of several subjects, and obtained satisfactory results. Fig. 6 shows representative correspondence-detection results. Four voxels in the same slice of model image are selected in Fig. 6(a). The corresponding voxels found from the subject image are shown in Fig. 6(b). Notably, voxels in the same slice of the model image do not necessarily have corresponding voxels in the same slice of the subject image. Therefore, different-sized crosses '+' are used to represent the slices of the detected corresponding voxels in the subject image. The smaller cross indicates that the corresponding voxel is above the current slice, while the larger cross indicates that the corresponding voxel is below the current slice.

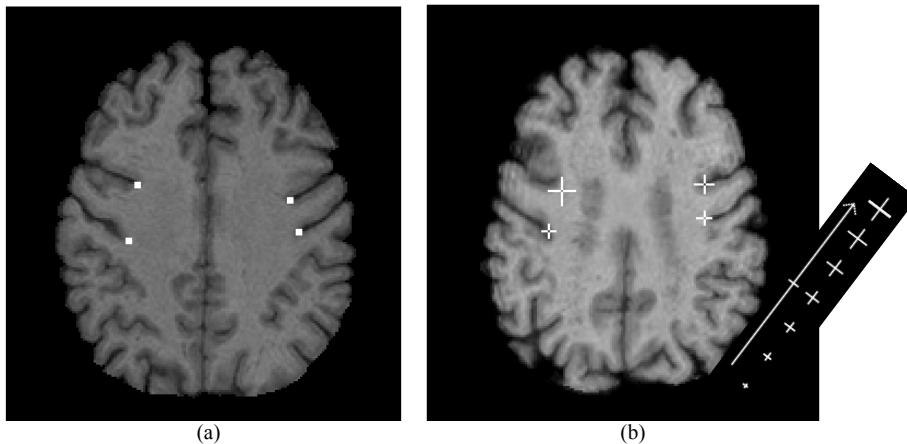


Figure 6. Examples of the results of correspondence detection. (a) Selected voxels at the same slice of model image; (b) the corresponding voxels found in the subject image. The medium-sized cross represents that the corresponding subject voxel is localized exactly at the current slice, while smaller and larger crosses represent that the corresponding subject voxels are found in the neighboring slices. The arrow indicates the increasing of the slice index.

4. MORPHOLOGICAL CLASSIFICATION OF BRAIN IMAGES

Information obtained through the analysis of brain images can be used to explain anatomical differences between normal and pathologic populations, and offers the potential to help in the early diagnosis of pathology. For example, subtle patterns of brain atrophy and changes in brain physiology in individuals with no clinical symptoms could prove to be predictors of the development of dementia at later stages. Interventions at early stages of a disease are often more effective than interventions at later stages. Therefore, developing methods for early diagnosis of subtle anatomical and physiological characteristics of populations bound to develop disease is becoming increasingly important, as pharmaceutical interventions are being developed concurrently.

Voxel- and deformation-based morphometry (VBM and DBM) using voxel-wise measurements have become common approaches to computational anatomy during the past several years [15,29,30]. The statistics of a morphological variable are determined for a normal population, and are compared against individual measurements or group statistics of another population (i.e., one with a particular disease). Voxels that display abnormal behavior are flagged and grouped into pathological regions. We present an approach that uses the entire set of morphological measurements obtained from all voxels in a brain image, to build a brain classifier [13]. Our classification scheme operates in a very-high-dimensional

space, and therefore can determine subtle population differences with complex spatial patterns, which often cannot be identified via voxel-wise statistical analysis.

Our approach is based on a mass-preserving framework called the Regional Analysis of Volumes Examined in Normalized Space (RAVENS) [31] and a high-dimensional elastic registration called Hierarchical Attribute Matching Mechanism for Elastic Registration (HAMMER) [32]. A RAVENS map is created by warping individual images into conformation with a template, while preserving the total amount of tissue in any brain region. Volume compression results in an increase of tissue density, so that the total amount of tissue is preserved. And similarly, volume stretching results in a decrease of tissue density. Regional volumetric analysis is performed by applying statistical analysis methods on the RAVENS tissue-density maps. Analysis of the RAVENS maps involves three major steps. First, we apply a wavelet decomposition to hierarchically decompose a RAVENS map in a scale-space way. Second, we use a feature selection method [11] to focus on the most discriminating aspects of the wavelet-transformed RAVENS maps. Third, we use the selected features and apply a Support Vector Machine (SVM) pattern recognition method [33] to achieve morphological classification.

Three experiments are used to demonstrate the performance of our approach. All testing images are obtained from the Baltimore Longitudinal Study of Aging study [2], where MR brain images of over 150 older adults have been collected yearly over nine years. We first applied the method to age classification. We divided 150 subjects into 4 age groups: 50~59, 60~68, 69~79, 80+, and tested our classification performance, using the leave-one-out method. The result in Fig. 7 shows that the most successful classification rate was achieved when comparing the most disparate age groups. The second experiment examined normal and pathology classification. We used 10 normal subjects and 10 subjects with simulated atrophy of different levels. For 5% atrophy, the leave-one-out classification rate was 95%, while at higher atrophy levels the leave-one-out classification rate was 100%. Our final experiment compared male and female brains, and resulted in a 98.9% classification accuracy, using the leave-one-out method.

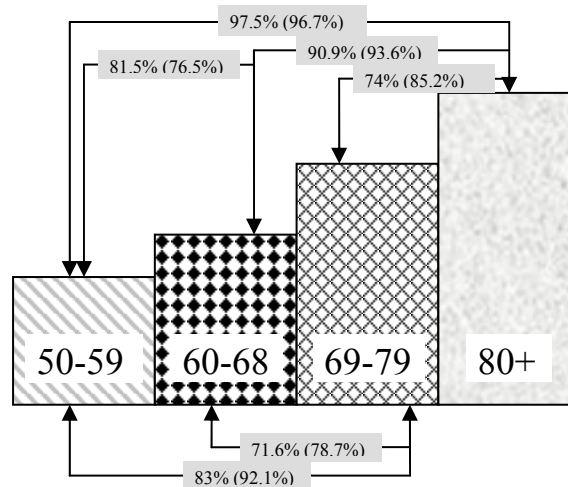


Figure 7. Morphological classification success rates for groups of different ages. The numbers in parentheses were obtained by using Year1 vs. Year5 longitudinal data, which in effect further separated the groups by 4 years.

5. CONCLUSION

We have presented three wavelet-based methods for application in the morphometric analysis of MR brain images. The first method uses wavelet transformation to hierarchically represent the shapes of the anatomical contours, thereby enabling the developed hierarchical ASM to capture a large range of shape variability even from a small group of training samples. The hierarchical ASM performs substantially better than the standard ASM even in the cases where as few as 5 training samples are used to model a 2D contour represented by 512 landmark points. Notably, the current

version of the hierarchical ASM was particularly designed for 2D contours. To apply the hierarchical ASM to the volumetric image segmentation, we must extend the current method for use on 3D surfaces. Our group is currently investigating this approach.

The second method focuses on using wavelet-based attribute vectors as morphological signatures of voxels for finding the anatomical correspondences among the brain images, which is a key step in image registration and shape analysis. Wavelets are employed to hierarchically characterize the anatomical structures in the vicinity of each voxel. We have validated this wavelet-based correspondence-detection algorithm on a large datasets, showing very promising results. Currently, we are applying this anatomical detection method to brain image registration/warping.

The third method uses wavelets to characterize the morphological measurements obtained from all voxels in a brain image, and then builds a brain classifier based on the entire set of wavelet coefficients. Besides the successful applications of this algorithm in sex, simulated pathology, and age classifications, we are currently applying this algorithm to differentiating the schizophrenic brain from the normal brain, using real data.

ACKNOWLEDGEMENT

We would like to thank Dr. Susan Resnick and the BLSA for providing the datasets, and Drs. Zhiqiang Lao and Zhong Xue for preparing the results in Figures 6 and 7.

REFERENCES

1. Sowell, E. R., Thompson, P. M., Holmes, C. J., Batth, R., Jernigan, T. L., and Toga, A. W., "Localizing age-related changes in brain structure between childhood and adolescence using statistical parametric mapping," *NeuroImage* vol. 9, pp. 587–597, 1999.
2. S. M. Resnick, A. Goldszal, C. Davatzikos, S. Golski, M. A. Kraut, E. J. Metter, R. N. Bryan, and A. B. Zonderman, "One-year age changes in MRI brain volumes in older adults," *Cereb. Cortex*, vol. 10, pp. 464–472, 2000.
3. C. Davatzikos, M. Vaillant, S. Resnick, J.L. Prince, S. Letovsky, and R.N. Bryan, "A Computerized Method for Morphological Analysis of the Corpus Callosum," *J. of Comp. Ass. Tomography*, vol. 20, pp. 88-97, Jan./Feb. 1996.
4. C. Davatzikos and S. M. Resnick, "Sex differences in anatomic measures of interhemispheric connectivity: correlations with cognition in women but not men," *Cerebral Cortex*, vol. 8, pp. 635-640, 1998.
5. C. Davatzikos, "Brain morphometrics using geometry-based shape transformations", in *Proc. of Workshop on Biomedical Image Registration*, Slovenia, August 1999.
6. Wright, I. C., McGuire, P. K., Poline, J.-B., Travers, J. M., Murray, R. M., Frith, C. D., Frackowiak, R. S. J., and Friston, K. J., "A voxel-based method for the statistical analysis of gray and white matter density applied to schizophrenia," *NeuroImage* vol. 2, pp. 244–252, 1995.
7. Woermann, F. G., Free, S. L., Koeppe, M. J., Ashburner, J., and Duncan, J. D., "Voxel-by-voxel comparison of automatically segmented cerebral grey matter—A rater-independent comparison of structural MRI in patients with epilepsy," *NeuroImage* vol. 10, pp. 373–384, 1999.
8. Paul M. Thompson, Tyrone D. Cannon, Katherine L. Narr, Theo van Erp, Veli-Pekka Poutanen, Matti Huttunen, Jouko Lönqvist, Carl-Gustaf Standertskjöld-Nordenstam, Jaakko Kaprio, Mohammad Khaledy, Rajneesh Dail, Chris I. Zoumalan, and Arthur W. Toga, "Genetic influences on brain structure," *Nature Neuroscience*, vol. 4, no. 12, pp. 1253-1258, Dec., 2001.
9. S. G. Mallat, "A theory for multiresolution signal decomposition: The wavelet representation," *IEEE Trans. Pattern Anal. Machine Intell.*, vol. 11, pp. 674–693, July 1989.
10. M. Lang, H. Guo, J. E. Odegard, C. S. Burrus, and R. O. Wells, "Noise reduction using an undecimated discrete wavelet transform," *IEEE Signal Processing Lett.*, vol. 3, pp. 10–12, Jan. 1996.
11. D. Shen and H. H. S. Ip, "Discriminative wavelet shape descriptors for invariant recognition of 2-D patterns," *Pattern Recogn.*, vol. 32, no. 2, pp. 151–165, Feb. 1999.
12. Z. Xue, D. Shen and C. Davatzikos, "Determining correspondence in 3D MR brain images using attribute vectors as morphological signatures of voxels", submitted to *IEEE Trans. on Medical Imaging*.

13. Z. Lao, D. Shen, and C. Davatzikos. "Morphological classification of brains via high-dimensional shape transformations and machine learning methods", submitted to *Neuroimage*.
14. Good, C.D., R.I. Scahill, N.C. Fox, J. Ashburner, et al., "Automatic differentiation of anatomical patterns in the human brain: Validation with studies of degenerative dementias". *Neuroimage*, 2002. **17**(1): p. 29-46.
15. Thompson, P.M., M.S. Mega, R.P. Woods, C.I. Zoumalan, et al., "Cortical Change in Alzheimer's Disease Detected with a Disease-specific Population-based Brain Atlas". *Cerebral Cortex*, 2001. **11**(1): p. 1-16.
16. M. Kass, A. Witkin, and D. Terzopoulos, "Snakes: Active contour models," *Int. J. Comput. Vis.*, vol. 1, no. 4, pp. 321-331, 1988.
17. D. Terzopoulos and D. Metaxas, "Dynamic 3D models with local and global deformations: Deformable superquadrics," *IEEE Trans. Pattern Anal. Machine Intell.*, vol. 13, pp. 703-714, July 1991.
18. L. H. Staib and J. S. Duncan, "Boundary finding with parametrically deformable models," *IEEE Trans. Pattern Anal. Machine Intell.*, vol. 14, pp. 1061-1075, Nov. 1992.
19. L. H. Staib and J. S. Duncan, "Model-based deformable surface finding for medical images," *IEEE Trans. Med. Imag.*, vol. 15, no. 5, pp. 720-731, 1996.
20. T. F. Cootes and C. J. Taylor, "Combining point distribution models with shape models based on finite element analysis," *Image Vis. Computing*, vol. 13, no. 5, pp. 403-409, 1995.
21. G. Szekely, A. Kelemen, C. Brechbuhler, and G. Gerig, "Segmentation of 2-D and 3-D objects from MRI volume data using constrained deformations of flexible Fourier contour and surface models," *Med. Image Anal.*, vol. 1, no. 1, pp. 19-34, 1996.
22. A. Kelemen, G. Szekely, and G. Gerig, "Elastic model-based segmentation of 3-D neuroradiological data sets," *IEEE Trans. Med. Imag.*, vol. 18, pp. 828-839, Oct. 1999.
23. D. Shen, E. Herskovits, and C. Davatzikos, "An adaptive-focus statistical shape model for segmentation and shape modeling of 3D brain structures," *IEEE Trans. Med. Imag.*, vol. 20, pp. 257-270, Apr. 2001.
24. D. Shen and C. Davatzikos, "An adaptive focus deformable model using statistical and geometric information," *IEEE Trans. Pattern Anal. Machine Intell.*, vol. 22, pp. 906-913, Aug. 2000.
25. N. Duta and M. Sonka, "Segmentation and interpretation of MR brain images using an improved knowledge-based active shape model," in *Information Processing in Medical Imaging*. Berlin, Germany: Springer-Verlag, 1997, pp. 375-380.
26. Y. Wang and L. H. Staib, "Boundary finding with prior shape and smoothness models," *IEEE Trans. Pattern Anal. Machine Intell.*, vol. 22, pp. 738-743, July 2000.
27. I. L. Dryden and K. V. Mardia, *Statistical Shape Analysis*. New York: Wiley, 1998.
28. C. Davatzikos, X. Tao and D. Shen, "Hierarchical Active Shape Models, Using the Wavelet Transform", *IEEE Trans. Med. Imag.*, vol. 22, no. 3, pp. 414-423, Mar. 2003.
29. Freeborough, P.A. and N.C. Fox, "Modeling brain deformations in Alzheimer's disease by fluid registration of serial 3D MR images". *J. Comp. Assist. Tomogr.*, 1998. **22**: p. 838-843.
30. J.C.Gee, "On matching brain volumes", *Pattern Recognition*, Vol.32, pp.99-111, 1999.
31. Goldszal, A.F., C. Davatzikos, D. Pham, M. Yan, et al., "An image processing protocol for the analysis of MR images from an elderly population". *J. Comp. Assist. Tomogr.*, 1998. **22**(5): p. 827-837.
32. D. Shen and C. Davatzikos. "Hammer: Hierarchical attribute matching mechanism for elastic registration." *IEEE Trans. Med. Imag.*, vol. 21, no. 11, pp. 1421-1439, Nov. 2002.
33. Burges, C.J.C., "A tutorial on support vector machines for pattern recognition". *Data Mining and Knowledge Discovery*, 1998. **2**(2): p. 121-167.